AD-A194 493 N2(A3EPSILON U+) BY REACTION OF N2F4 + H2 IN A SUPERSONIC FLOW(U) AIR FORCE WEAPONS LAB KIRTLAND AFB NM Y D JONES ET AL. MAR 88 AFWL-TR-87-73 1/1

UNCLASSIFIED F/G 9/3 NL

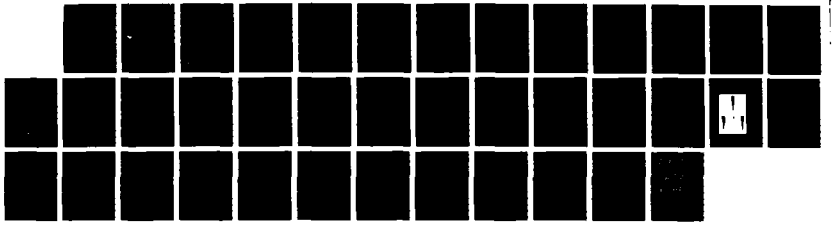

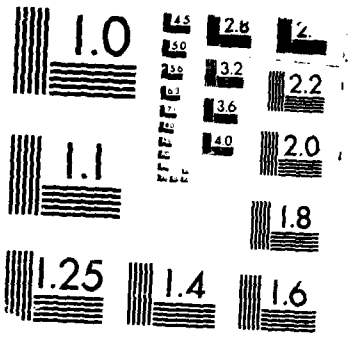

MICROCOPY RESOLUTION TEST CHART

BUREAU OF STANDARDS-1963-A

AFWL-TR-87-73

AFWL-TR-
87-73

$N_2(A^3\Sigma u^+)$ BY REACTION OF $N_2F_4 + H_2$ IN A SUPERSONIC FLOW

Y. D. Jones
N. D. Founds
D. V. Hibson
M. R. Palmer

March 1988

Final Report

AIR FORCE WEAPONS LABORATORY
Air Force Systems Command
Kirtland Air Force Base, NM 87117-6008

UNCLASSIFIED
SECURITY CLASSIFICATION OF THIS PAGE

REPORT DOCUMENTATION PAGE

1a. REPORT SECURITY CLASSIFICATION Unclassified	1b. RESTRICTIVE MARKINGS
2a. SECURITY CLASSIFICATION AUTHORITY	3. DISTRIBUTION / AVAILABILITY OF REPORT Approved for public release; distribution unlimited.
2b. DECLASSIFICATION / DOWNGRADING SCHEDULE	
4. PERFORMING ORGANIZATION REPORT NUMBER(S) AFWL-TR-87-73	5. MONITORING ORGANIZATION REPORT NUMBER(S)
6a. NAME OF PERFORMING ORGANIZATION Air Force Weapons Laboratory 6b. OFFICE SYMBOL (If applicable) ARBL	7a. NAME OF MONITORING ORGANIZATION
6c. ADDRESS (City, State, and ZIP Code) Kirtland Air Force Base, New Mexico 87117-6008	7b. ADDRESS (City, State, and ZIP Code)
8a. NAME OF FUNDING / SPONSORING ORGANIZATION 8b. OFFICE SYMBOL (If applicable)	9. PROCUREMENT INSTRUMENT IDENTIFICATION NUMBER
8c. ADDRESS (City, State, and ZIP Code)	10. SOURCE OF FUNDING NUMBERS PROGRAM ELEMENT NO. 62601F; PROJECT NO. 3326; TASK NO. 03; WORK UNIT ACCESSION NO. 85

11. TITLE (Include Security Classification)
$N_2(A^3\Sigma u^+)$ BY REACTION OF $N_2F_4 + H_2$ IN A SUPERSONIC FLOW

12. PERSONAL AUTHOR(S)
Jones, Y.D.; Founds, N.D.; Hibson, D.V.; and Palmer, M.R.

13a. TYPE OF REPORT	13b. TIME COVERED	14. DATE OF REPORT (Year, Month, Day)	15. PAGE COUNT
Final	FROM Jul 84 TO Feb 86	1988, March	42

16. SUPPLEMENTARY NOTATION
Tetrafluorohydrazine diatomic hydrogen deuterium diatomic nitrogen

17. COSATI CODES		
FIELD	GROUP	SUB-GROUP
07	02	
09	03	

18. SUBJECT TERMS (Continue on reverse if necessary and identify by block number)
Nitrogen fluorides, Chemical lasers, Nitrogen trifluoride, Metastable nitrogen, Excited nitrogen.
a 1 Delta b 1 Sigma

19. ABSTRACT (Continue on reverse if necessary and identify by block number)

The $N_2F_4 + H_2(D_2)$ reaction has been used to produce $NF(a^1\Delta)$ and $NF(b^1\Sigma)$ in supersonic flow. The extension of that reaction sequence in excess hydrogen is that $N_2(B)$ is produced which relaxes to the $N_2(A)$ electronic state with an energy content of 6.2 eV. The energy storage potential of $N_2(A)$ and subsequent transfer of energy to other molecules, such as NO, SO and IF, makes this production method of extreme interest for laser applications. The device diagnostics, parametric studies and final yield of $N_2(A)$ are described. The yield of $N_2(A)$ is lower than expected from subsonic studies, but the experiments indicate areas of study required to understand the system in greater detail.

Keywords: Metastable state; Excitation

20. DISTRIBUTION / AVAILABILITY OF ABSTRACT	21. ABSTRACT SECURITY CLASSIFICATION
☐ UNCLASSIFIED/UNLIMITED ☒ SAME AS RPT. ☐ DTIC USERS	Unclassified
22a. NAME OF RESPONSIBLE INDIVIDUAL Nanette D. Founds	22b. TELEPHONE (Include Area Code) (505) 844-0196
	22c. OFFICE SYMBOL AFWL/ARBL

DD FORM 1473, 84 MAR 83 APR edition may be used until exhausted. All other editions are obsolete.

SECURITY CLASSIFICATION OF THIS PAGE
UNCLASSIFIED

ACKNOWLEDGEMENT

The authors would like to thank TSgt James E. Garrett II, Richard J. Barber, Roman L. Martinez, Michael L. Orbock and Robert Hughes for their dedication to the project, their support of the facility, and its operation. We would also like to thank Don Vonderhaar for his tremendous design effort on the device cavity.

CONTENTS

FIGURES

1.0 INTRODUCTION

Excited nitrogen has been of major interest for many years because of its highly energetic metastable states (Refs. 1 to 5). The most used method for production of the first excited electronic state of N_2 has been by electrical discharge excitation of Ar and subsequent transfer to N_2 to form $N_2(A^3\Sigma^+U)$ (Ref. 2). The $N_2(A)$ molecule contains 6.2 eV of energy which allows for a transfer to molecules that are better suited to lasing than N_2 such as NO, SO and IF. The 2.0 s lifetime of the $N_2(A)$ state makes it unsitable for lasing. A purely chemical generation method for $N_2(A)$ has not previously been shown to produce high densities of the excited state.

This study determined what densities of $N_2(A)$ could be produced using NF_2 + H_2 by the following basic reactions:

$$N_2F_4 \xrightarrow{\Delta} NF_2 \quad (1)$$

$$F + H_2 \rightarrow H + HF \quad (2)$$

$$H + NF_2 \rightarrow NF(a^1\Delta) + HF \quad (3)$$

$$H + NF(a^1\Delta) \rightarrow N(^2D) + HF \quad (4)$$

$$N(^2D) + NF(a^1\Delta) \rightarrow N_2(B) + F \quad (5)$$

$$N_2(B) \rightarrow N_2(A) + h\nu \quad (6)$$

A more detailed reaction scheme is given in the Appendix. The study was performed in supersonic flow to minimize the operating gas phase temperature and provide preliminary information on $N_2(A)$ in a possible lasing media. Previous work indicated that this reaction sequence in a subsonic flow tube produced excited N_2 (Ref. 3). However, the reaction had not been used to produce densities greater than 10^8 molecules/cc in the flow tube low pressure condition.

2.0 DEVICE DESCRIPTION

2.1 OVERVIEW

The overall experimental system consisted of a 316L stainless steel chamber with viewing ports on four sides. Figure 1 shows a view of the chamber with positions shown for the gas input plumbing. The chamber was exhausted into a cooled diffuser in the transition section and two heat exchangers. The device was evacuated using two Kinney 850 cfm pumps with two M&D Pneumatics 2700 cfm blowers for a system total of 7,100 cfm.

The BCL-16 nozzle was positioned on the chamber wall with the gas inputs. The BCL-16 nozzle cross section in shown in Fig. 2. The nozzle and flow systems have been discussed in detailed in previous reports (Refs. 4, 5). The BCL-16 nozzle was developed for HF/DF laser application (Ref. 4) and studied for those same systems (Ref. 6). For the $N_2F_4 + H_2$ system the combustor portion of the assembly nozzle was operated at design conditions to profuce F atoms. The hydrogen or deuterium and fluorine were injected into the combustor along with He diluent at a molar ratio of F_2: D_2: He of approximately 1:2:50.

The combustor portion of the nozzle was N_2-cooled by an external copper collar around the body of the combustor. The internal temperature of the combustor was maintained by using a Ni liner with an air gap between the outer diameter of the liner and inner diameter of the combustor wall. This configuration was determined by extensive testing with LaB_6 and alumina liners. The LaB_6 and alumina liners failed after minimal usage. The result was that debris from the liners plugged the primary nozzles preventing further operation. The Ni liner lasted over 10 test sequences. A study of the mixing performance of the BCL-16 nozzle was performed under reactive conditions. The preliminary summary of the study will be presented under the Results section of this report.

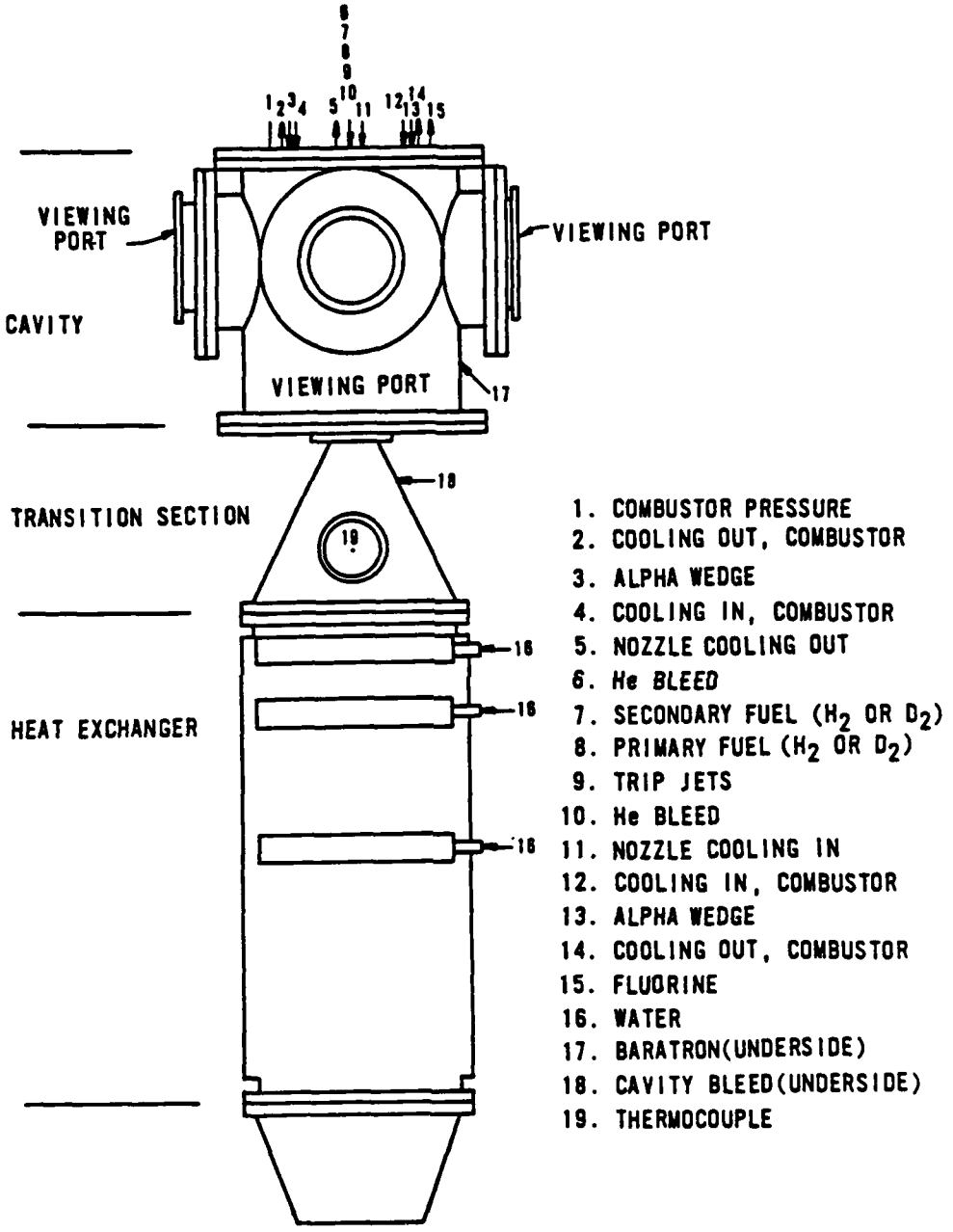

Figure 1. Device schematic.

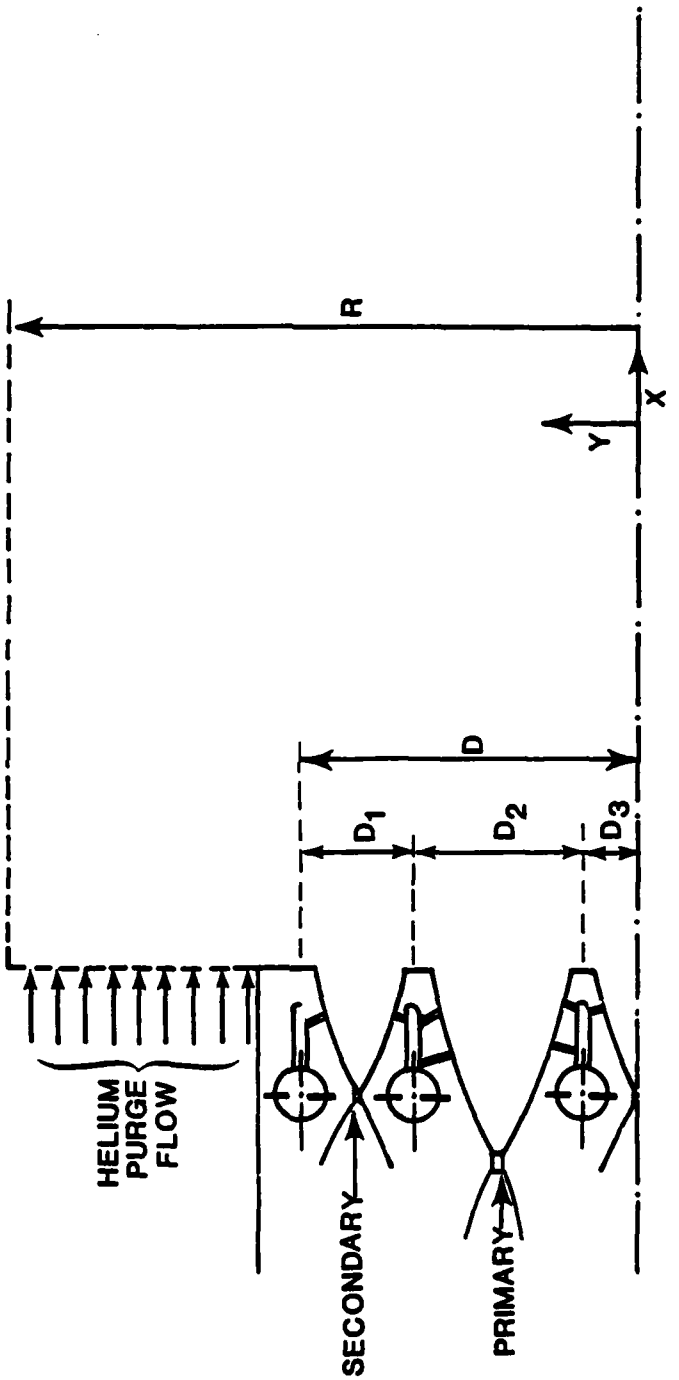

Figure 2. BCL-16 nozzle.

3.0 DIAGNOSTICS

3.1 $NF(a^1\Delta)$ AND $NF(b^1\Sigma)$ EMISSION MEASUREMENT

The $NF(a^1\Delta)$ diagnostic was an extremely important part of the device performance analysis and has been descibed previously (Ref. 7). The overall arrangement of the NF(a) and NF(b) diagnostics is shown in Fig. 3. The 874.2 nm emission from the NF(a-X) transition was detected via a 38.1 cm long spatial filter with 0.17 cm-dia orifices coupled to a fused silica fiber optic. The fiber optic was bifurcated so that one end was fed into the NF(b) diagnostic, which monitored the NF(b-X) transition at 528.8 nm. The allowed simultaneous detection of NF(a) and NF(b) within the same viewing volume. The flame shape was photographed and digitized to determine the actual viewing volume (Fig. 4).

Errors for the diagnostics were based upon the extent of interferences from other emissions, uncertainties in the liftimes and calibration errors. The error for the $NF(b^1)$ diagnostic was determined to be ±10% with a range of 10^{11} to 10^{13} molecules/cc. For the $NF(a^1\Delta)$ diagnostic, the error was larger because of the interferences from other emissions in the system and was estimated at ±20% with a range of 10^{14} to 10^{16} molecules/cc.

The spatial filter was mounted on a remotely operated translation stage with a linear voltage displacement transducer (LVDT) to accomplish scans across the centerline of the flow field of the device with a known position. Sample scans of the $NF(a^1\Delta)$ and $NF(b^1\Sigma)$ emissions are shown in Figs. 5 and 6. Scans were made starting at the nozzle exit plane (NEP). The scan was not begun until all flows were stable.

3.2 OPTICAL MULTICHANNEL ANALYZER (OMA)

The OMA III 1460R system (EG&G PAR) was used to monitor the change in emission over a wide wavelength range (usually 300-900 nm) at a fixed point within the device. The OMA III system and its calibration has been described in Ref. 5. This diagnostic was only used to determine volume-averaged changes of the excited state production in the device with respect to flow rate changes.

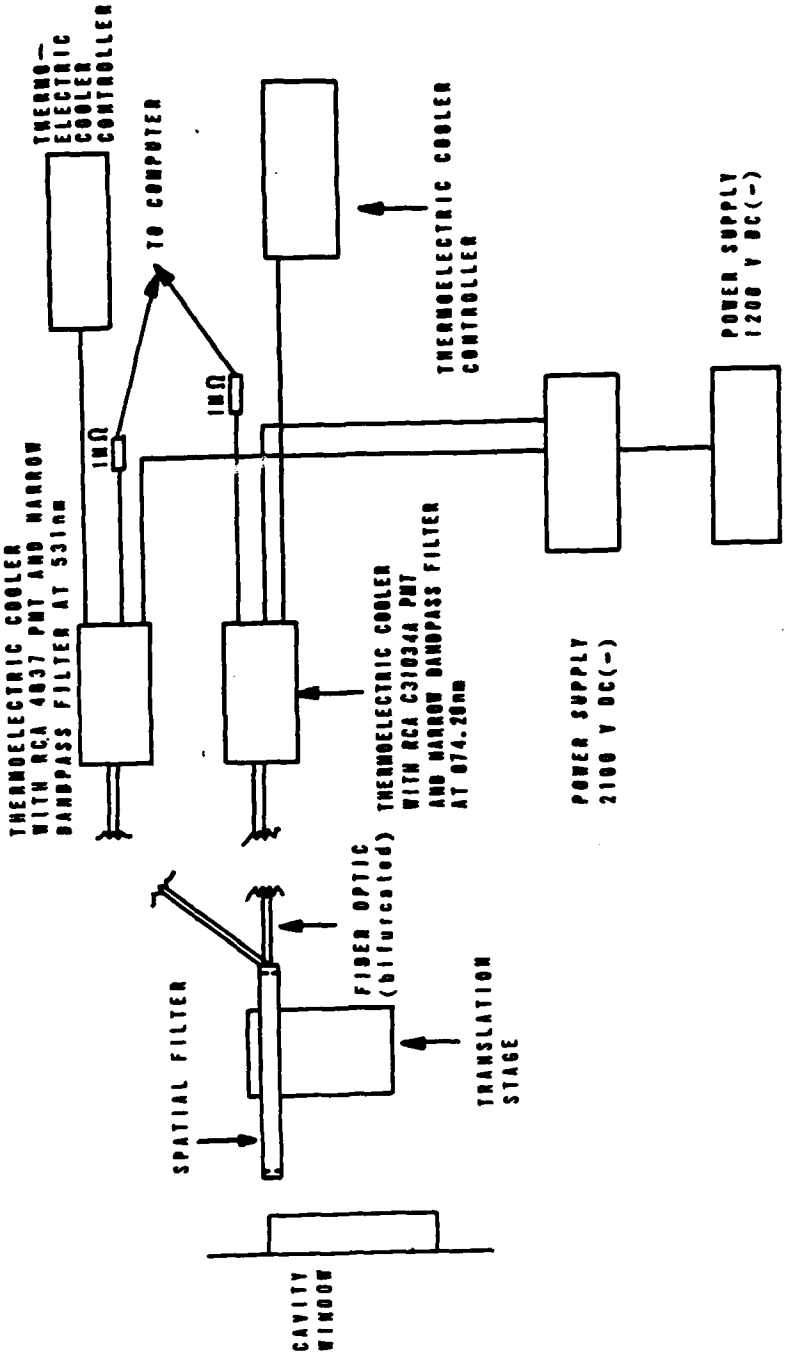

Figure 3. NF(a) and NF(b) diagnostic schematic.

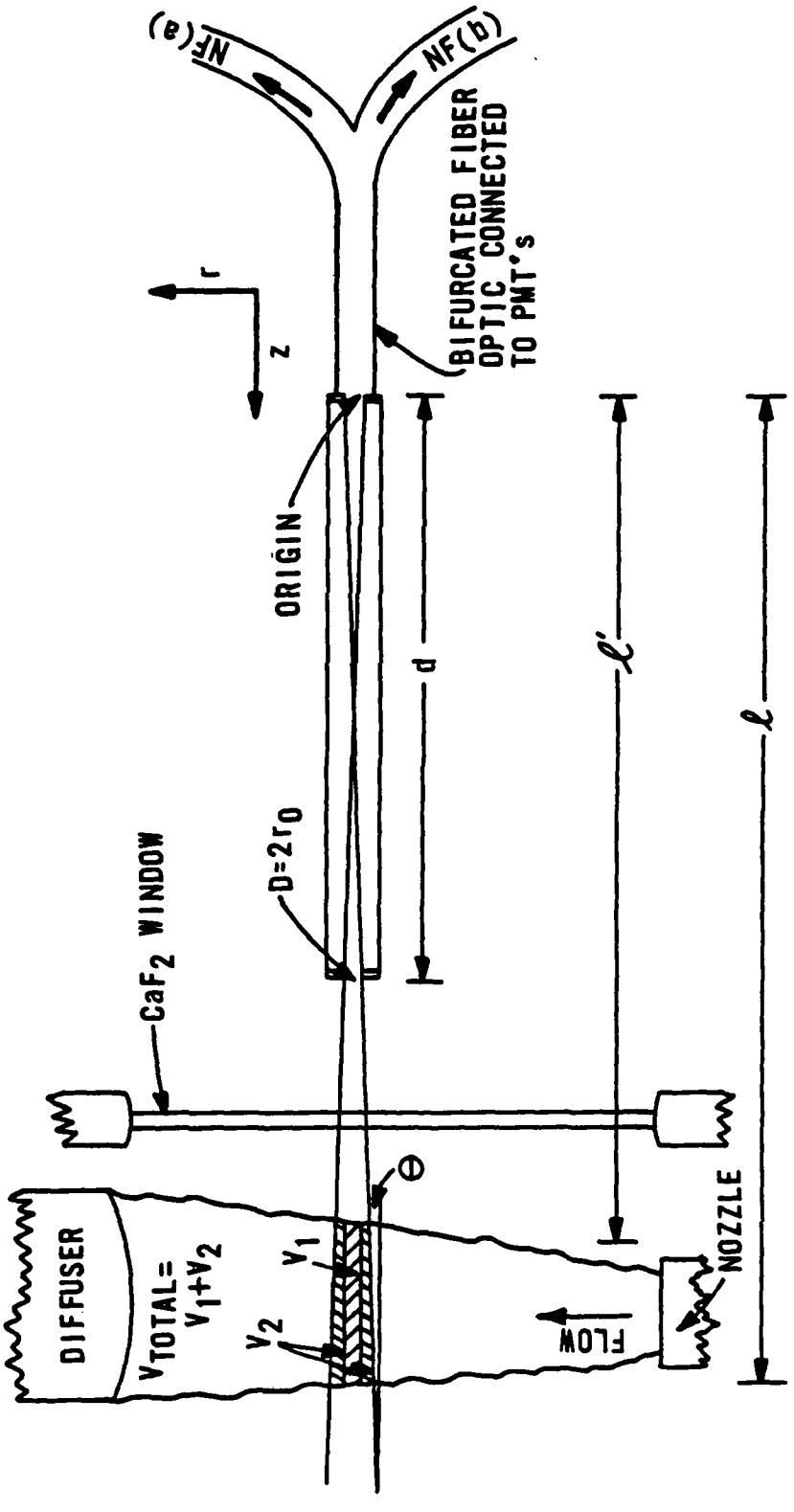

Figure 4. Experimental arrangement of diagnostics.

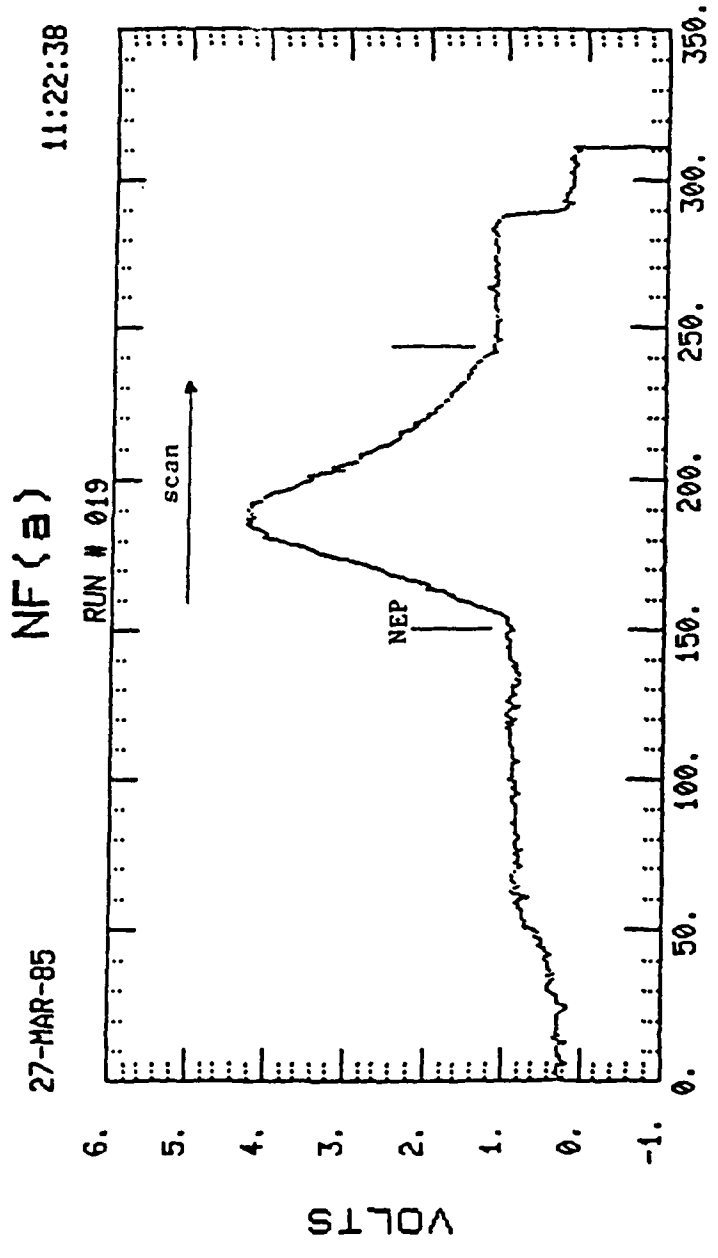

Figure 5. NF(a) sample scan.

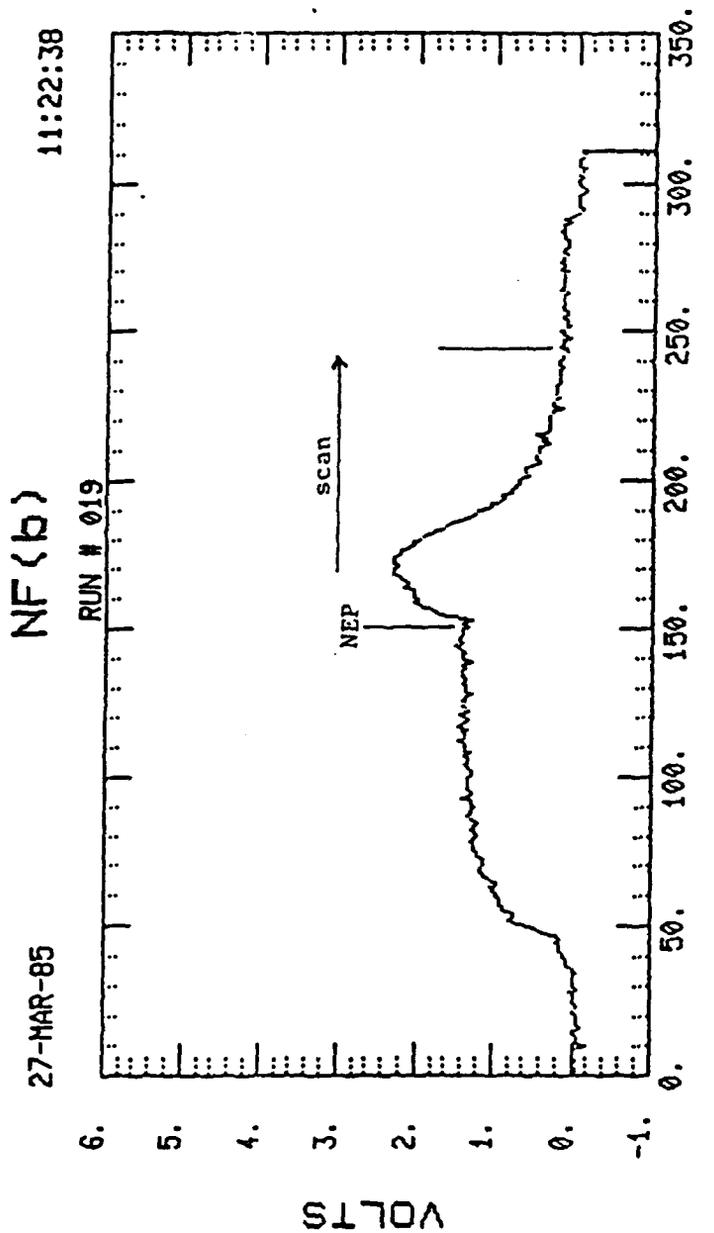

Figure 6. NF(b) sample scan.

4.0 INFRARED EMISSION MEASUREMENTS

4.1 $N_2(B^3\Pi g)$

To determine the contribution to the total $N_2(B)$ population by the infrared (IR) vibrational transitions, a 0.3 m monochromator (Acton) equipped with a 1.0 μm blazed, 1200 l/mm grating was used. The emission was collected using a fused silica fiber optic which was rectangular on one end to match the monochromator slit. The collection volume was defined by a spatial filter. Scans from 900 nm to 1.5 μm were performed at a fixed point in the middle of the flow. The diagnostic used an intristic Ge detector (Applied Detector Corporation, Model 403L). The entire diagnostic was calibrated using a FEL-type standard lamp (Eppley Laboratories) and with a blackbody (Infrared Industries Inc.). The number density was compared to the $N_2(B)$ visible emission measured at the same point in the flow using the calibrated OMA III. The $N_2(B)$ population could be determined to within ±15%.

4.2 HF AND DF

Vibrationally excited HF and DF were produced in the combustor and in subsequent reactions of NF_2. The rotational distribution of the HF(DF) produced was of interest in terms of evaluating possible interference with other diagnostics and in determining the gas phase temperature assuming rotational equilibrium. The HF(DF) emission was studied with the OMA III to its limit of 900 nm. Further into the IR, HF(DF) emission was examined using the 0.3 m monochromator and detector described in the previous paragrah. A 3.0 μm blazed grating was used. Only relative peak heights were of interest from this diagnostic.

5.0 ULTRAVIOLET (UV) DIAGNOSTICS

5.1 $N_2(C)$

The $N_2(C-B)$ emission is due to the creating of the C state from $N_2(A)$ pooling as given by

$$2\ N_2(A^3\Sigma_u^+) \rightarrow N_2(C^3\pi_u) + N_2(X^1\Sigma_g^+) \qquad (7)$$

The rate for the pooling reaction is very fast, 1.0 to 2.6 x 10^{-10} cm^3/molecule-s (Ref. 8), ultimately determining the maximum $N_2(A)$ concentration which may be produced. The lifetime of the $N_2(C)$ state is 3.92 x 10^{-8} (Ref. 9). Knowing the pooling rate, the $N_2(A)$ concentration may be calculated from a known $N_2(C)$ number density. This diagnostic was used as a cross-check on $N_2(A)$ densities determined by $N_2(B-A)$ emission. Contaminants in the N_2F_4 lead to NO emission interferring with many of the known $N_2(C)$ peaks during experimental testing.

The apparatus used was a 1.0 m vacuum ultraviolet (VUV) monochromator (Acton) equipped with MgF_2 windows. Scans were performed from 250 to 400 nm using a fused silica fiber optic. The detection was via a Hamamatsu R928 photomultiplier tube (PMT). Calibration was performed using the FEL-type standard lamp and narrow bandpass filters to determine the systems response at specific wavelengths. Blocking filters were used to minimize interference from UV scatter. The OMA III system was used to confirm peaks at wavelengths greater than 300 nm. Because of the large interference from NO(A-X) emission in the US, this diagnostic was less accurate than measurement of $N_2(B)$. The $N_2(C)$ population could be determined to within ±30%.

6.0 GAS PHASE TEMPERATURE DETERMINATION

Scans of the HF rotational distribution were performed on several representative tests. The relative intensity plotted versus J(J + 1) yields a gas phase temperature for that area of the flow field. Scans were performed using the apparatus as described in the IR emission section. The HF(0-1) data were rejected because of self-absorption. Temperatures in the flow field ranged from 1200 to 1600 K. Use of the Boltzmann distribution to determine gas phase temperature asseumes an equilibrium exists. Errors because of nonequilibrium as well as some self-absorption are estimated at 200 percent.

7.0 PARAMETRIC FLOW STUDIES

Extensive flow variation studies were performed with the BCL-16 nozzle. The purpose of the flow studies was to begin with a computer-modeled set of combustor conditions and optimize the combustor performance. One the combustor was optimized and, thus, the F production, the H_2 (or D_2) and NF_2 were varied to optimize N_2(B-A) emission. To optimize to combustor, actual H atom production was monitored. Hydrogen was added through the secondary jets and NO added through the trip jets. The H + NO reaction produces a red emission from the relaxation of excited HNO which is formed. The gas phase titration to determine the H atom level has been described in Ref. 5.

The next series of tests involved setting the reagent flows at a computer-modeled set of conditions and optimizing one reagent at a time. Once a specific flow was optimized the other flows were one at a time varied to achieve the highest N_2(B) level. Then the original reagent flow was checked to ensure maximum intensity. Figures 7 through 9 show samples from the test series. The N_2(B-A) emission appeared to be relatively insensitive to most flows except N_2F_4 and F_2. Even the response to N_2F_4 flow change was smaller than might be anticipated (Fig. 9).

One series of tests were designed to determine if by using D_2 in place of H_2 in the secondary jets, the NF(b) production could be minimized as a parasitic pathway and, thus, N_2(B-A) increased. The overall result was that with D_2 the N_2(B) number density increased from 5 to 10 times the $[N_2(B)]$ previously achieved with H_2. The increase may be also because of improved mixing from increased penetration of the jets -- the jet penetration being dependent upon the molecular weight of the gas. The decoupling of the chemistry and mixing issues has not been completed; however, some investigation of the mixing in the BCL-16 nozzle was performed. The method used is discussed in Ref. 6. A sheet of Ar^+ laser light, 514.5 nm was directed into the device. The 514.5 nm wavelength excites I_2 that is injected through each set of jets, such as primary, secondary or trip, at separate times. The fluorescence is then photographed as the sheet of light is translated across the NEP. A

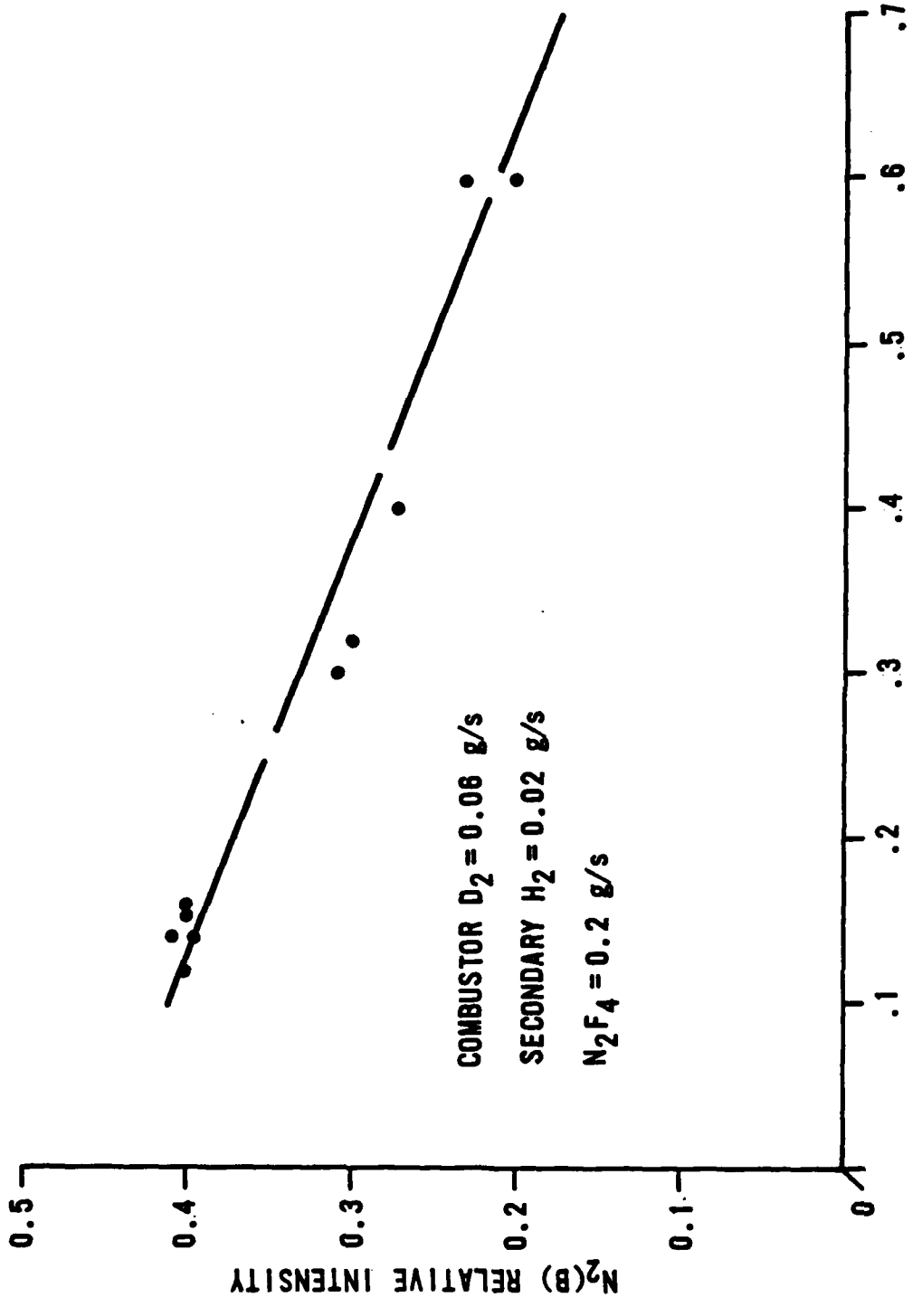

Figure 7. $N_2(B)$ variation with F_2.

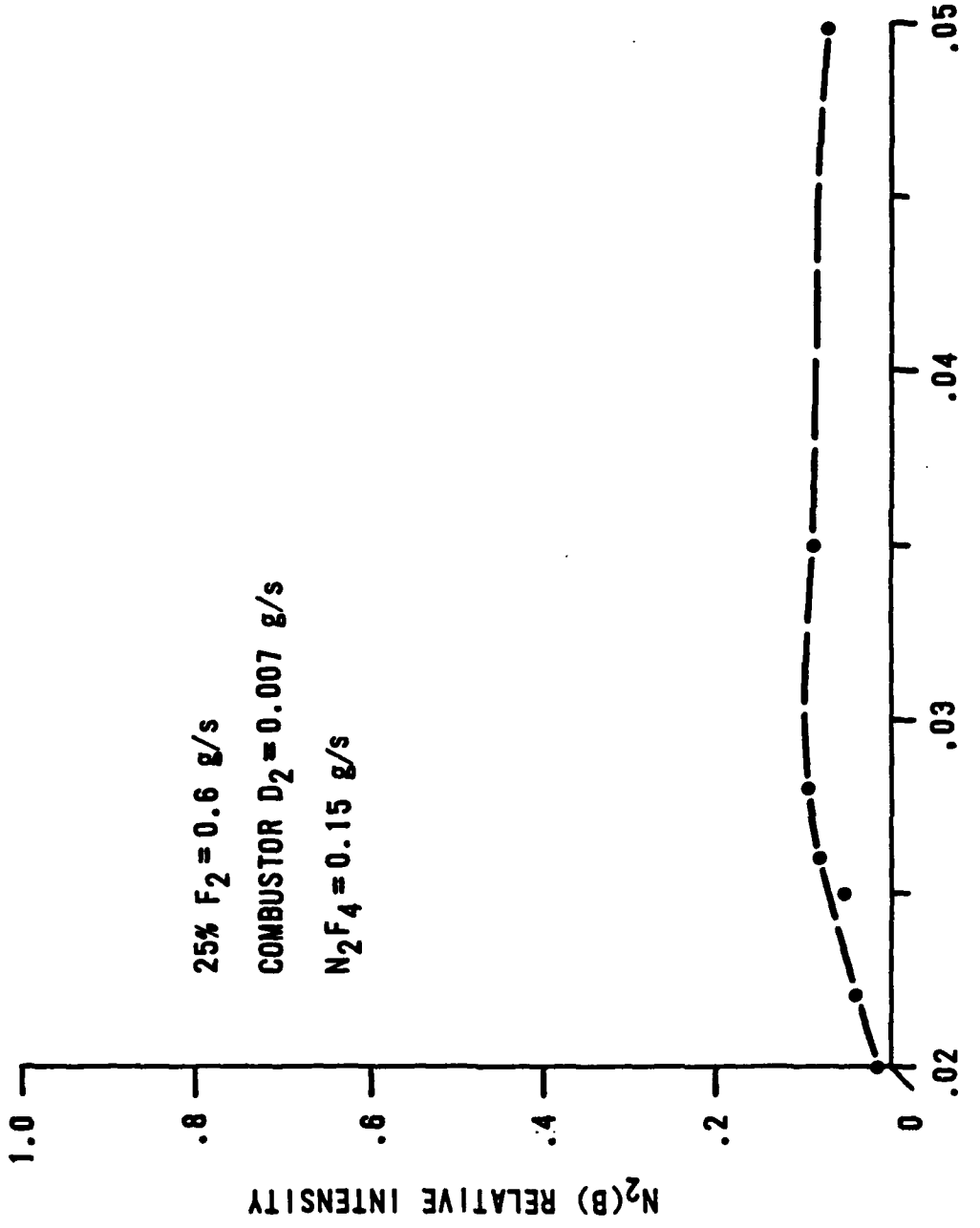

Figure 8. N_2(B) variation with secondary H_2.

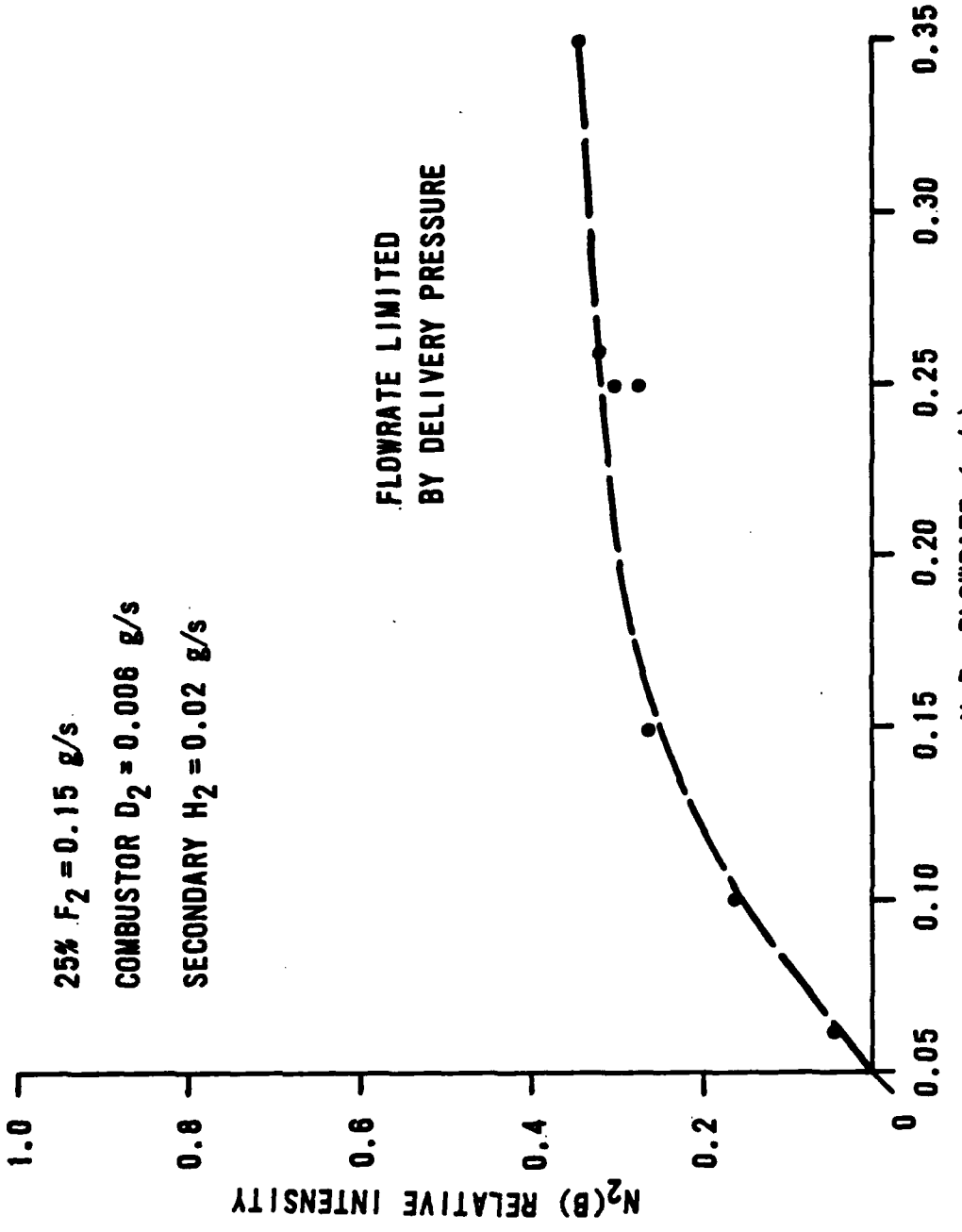

Figure 9. N_2(B) variation with N_2F_4.

diagram of the experimental setup is shown in Fig. 10. The photographs from each set of jets were digitized and combined to determine the over-lap areas. The area of overlap indicates where the jets are mixing. Care was taken to use inert carrier gases which would be similar to the molecular weight of the actual reactive flow gases. Figure 11 shows the result of the photograph overlapping at one position in the flow field. The area of overlap is small indicating poor mixing. The quantitative effect is not easily determined by these cold flow investigations. The cold flow studies do indicate, however, that mixing is a significant factor causing low $N_2(A)$ production.

Table 1 gives a set of sample test conditions which yielded high $N_2(B)$ number densities and compare D_2 versus H_2 secondary injection. The concentrations of $NF(a^1\Delta)$ and $NF(b^1\Sigma)$ are given in addition to the $N_2(B)$ concentrations. The $NF(a^1\Delta)$ and $NF(b^1\Sigma)$ concentrations are peak values taken from the scanning diagnostic, whereas the $N_2(A)$ concentration is volume averaged over a larger portion of the flame.

The $N_2(A)$ yield calculated from the maximum production set of flow rates (using $N_2(B)$ populations) and based upon initial N_2F_4 flow is 10^{-3}%. The flow rates for this case are listed first in Table 1. The yield of $NF(a^1\Delta)$ is also lower than predicted from earlier studies (Ref. 10). The yield for $NF(a^1\Delta)$ never exceeded 35 percent in any test sequence. This indicated the branching ratio might also not be correct. Flow tube studies were performed in this laboratory which confirmed the branching ratio might indeed be on the order of 35 percent to $NF(a^1\Delta)$.*

To confirm that the $N_2(A)$ popoulation was represented by the $N_2(B)$ visible emission as shown in a sample OMA III scan (Fig. 12), the IR portion of the $N_2(B)$ emission was examined. The prominent features of the $N_2(B)$ spectrum are the 1-0, 0-0 and 0-1 peaks between 850 and 1250 nm. The only peak which was

*Communication with Dr. Miles R. Palmer regarding a forthcoming publication, Sept 1986.

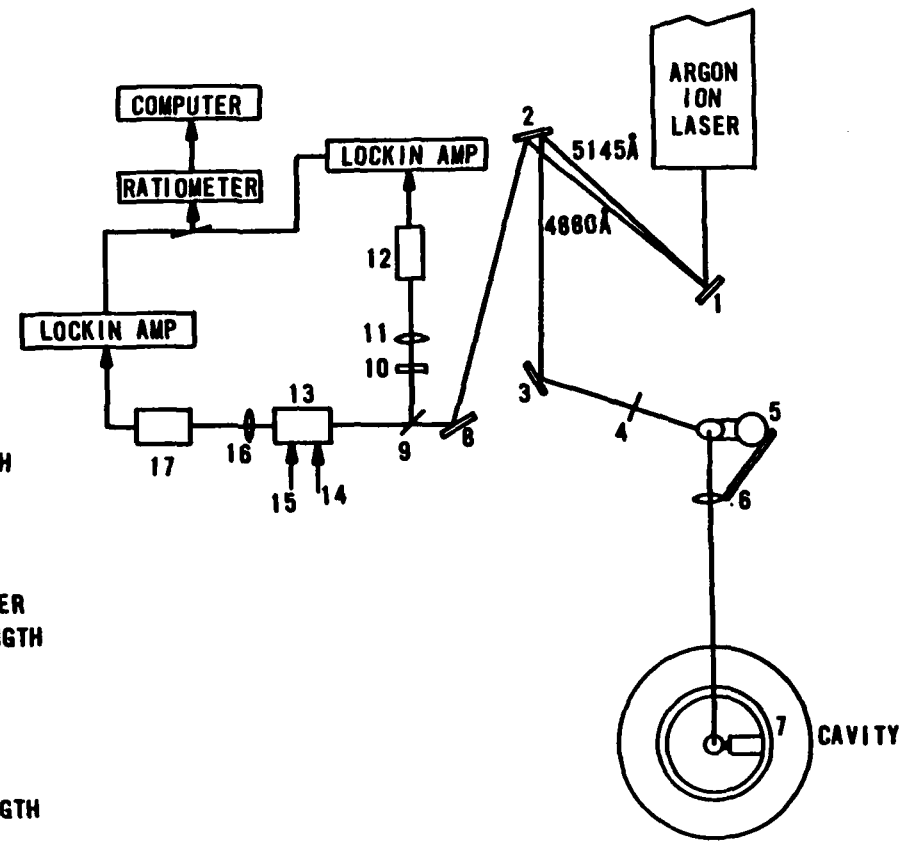

1. GRATING
2. MIRROR
3. MIRROR
4. IRIS DIAPHRAGM
5. BEAM STEERER
6. LENS; 1m FOCAL LENGTH
7. RASTER MIRRORS
8. MIRROR
9. BEAM SPLITTER
10. NEUTRAL DENSITY FILTER
11. LENS, ~7cm FOCAL LENGTH
12. Ge PHOTODIODE
13. I_2 CELL
14. PRESSURE TRANSDUCER
15. THERMOCOUPLE
16. LENS, ~7cm FOCAL LENGTH
17. Ge PHOTODIODE

Figure 10. LIF apparatus schematic.

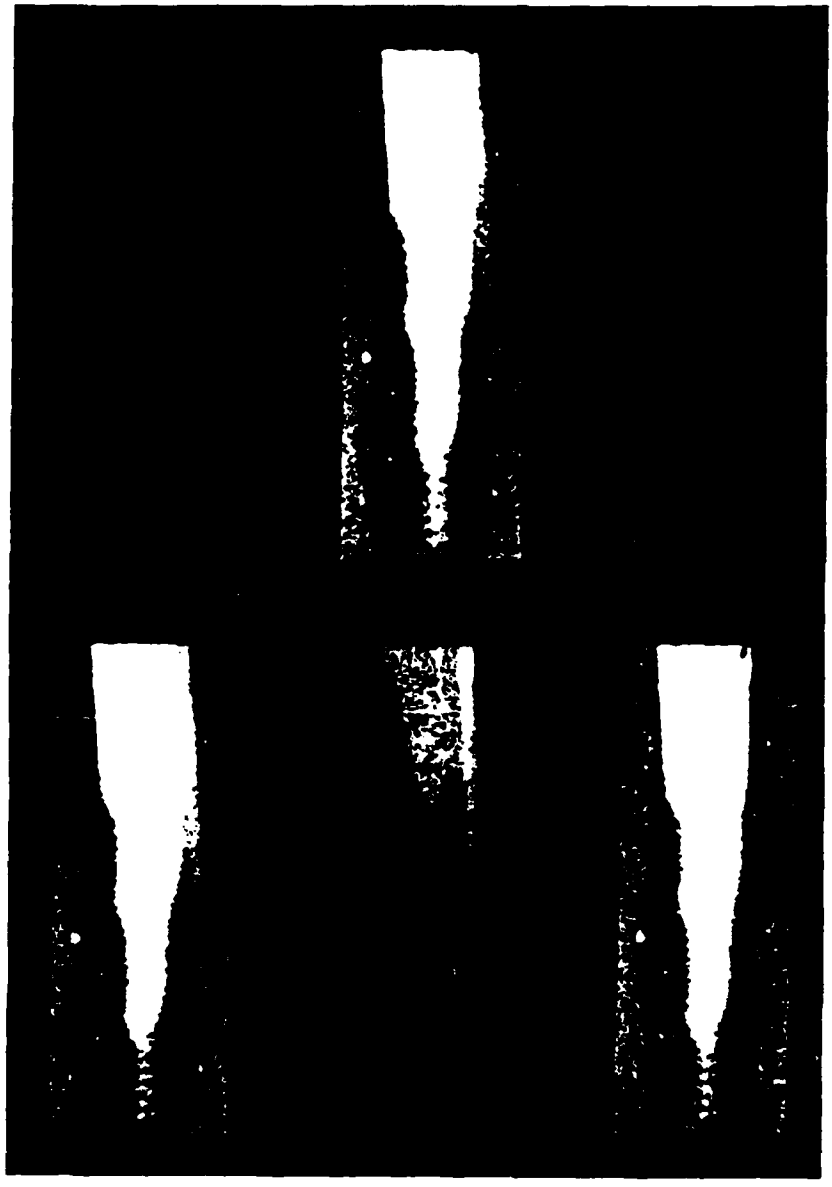

Figure 11. Computer generated images from the laser induced fluorescence (LIF) photographs.

TABLE 1. Sample comparisons of H_2 and D_2 secondary injection.

Primary[a]		Secondary[a]				(molecules/cm^3)			Test
25% F_2 in He	D_2	D_2 or H_2	He	Trip[a] N_2F_4	P_{cavity} (torr)[b]	$N_2(A)$	$NF(a^1\Delta)$	$NF(b^1\ )$	Run
0.156	0.0063	0.011 H_2	0.025	0.25	9.4	9.3×10^{9}	2.0×10^{15}	2.4×10^{12}	24-10
0.151	0.0066	0.020 D_2	0.025	0.25	10.3	5.8×10^{10}	4.0×10^{15}	1.5×10^{12}	25-5
0.156	0.0063	0.013 H_2	0	0.25	9.4	1.1×10^{10}	6.7×10^{15}	3.3×10^{12}	24-9
0.154	0.0078	0.021 D_2	0	0.26	13.7	1.6×10^{10}	9.6×10^{10}	1.4×10^{12}	26-4

[a]All flow rates are in g/s.

[b]Torr = 1.33×10^2 Pa.

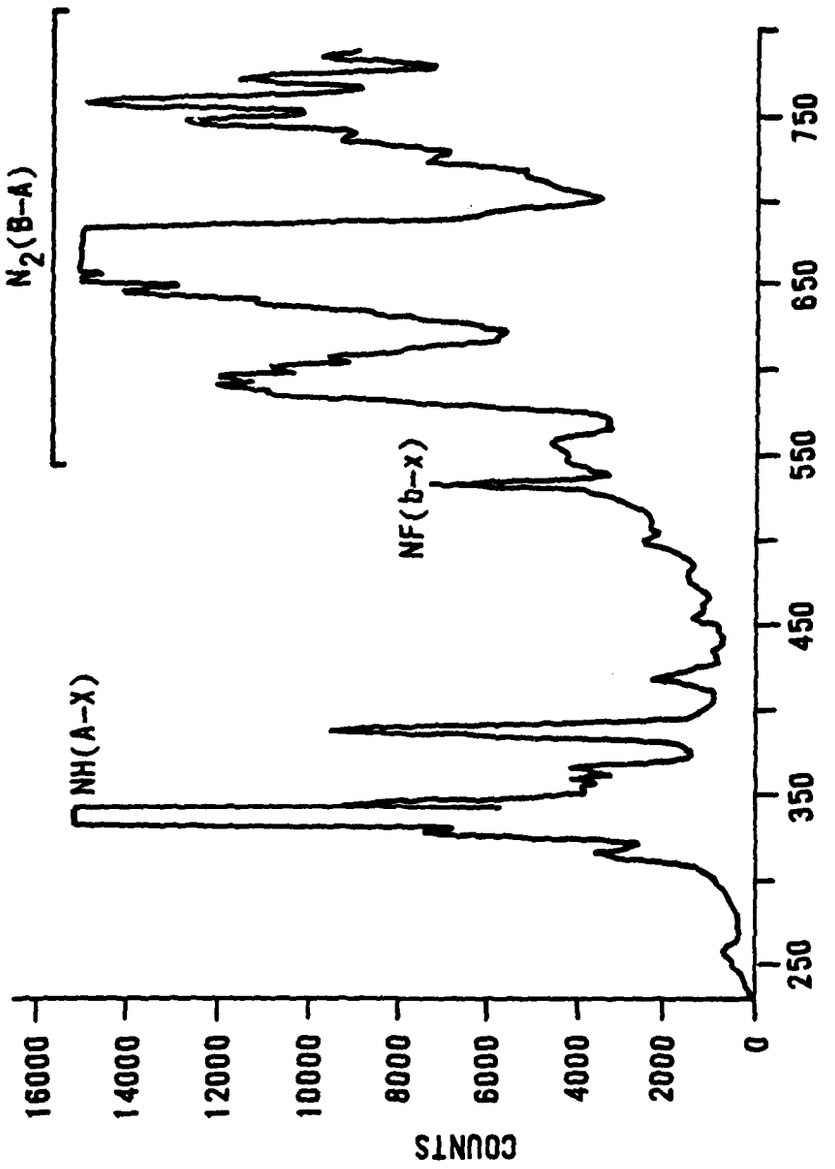

Figure 12. OMA III spectrum.

detected in the scans on the device was the 0-0 transition at 1050 nm. Population attributed to the 0-0 peak was only 1.3 percent of the total population in the 450-850 nm transitions levels. Therefore, it was concluded that the use of the visible emission to determine the $N_2(B)$ total population was a credible method. Scans in the UV were used to determine if the $N_2(C)$ population indicated the same $N_2(A)$ concentration as the $N_2(B)$ emission. $N_2(A)$ was looked for directly as well. The NO(A-X) emission swamped all efforts to observe $N_2(A)$ directly. Two $N_2(C)$ peaks were identified in the 310 to 320 nm region. These are indicated in Fig. 13, which shows a trace of one of the UV scans.

Calculating the population from the $N_2(C)$ 2-1 and 1-0 peaks and assuming the vibrational distribution is known (Ref. 11), the total $N_2(C)$ population is estimated to be 6×10^5 molecules/cc. This yields a $N_2(A)$ concentration of 2.4×10^{11} molecules/cc by employing the rate for Equation 7 since

$$[N_2(A)] = \left([N_2(C)]/k_p\tau_C\right)^{\frac{1}{2}} \tag{8}$$

where k_p is the pooling rate, and τ_C is the radiative lifetime of the $N_2(C)$ state ($\tau_C = 3.99 \times 10^{-8}$ s). This result compared well with the $N_2(B)$ emission of 1.6×10^{11} molecules/cc for the same test. With the assumptions made regarding vibrational distribution of $N_2(C)$ population, the only confirmation required is that of order of magnitude; this was accomplished. It is, therefore, accurate to determine the $N_2(A)$ population based upon $N_2(B)$ visible emission in the apparatus and flow conditions used in these experiments.

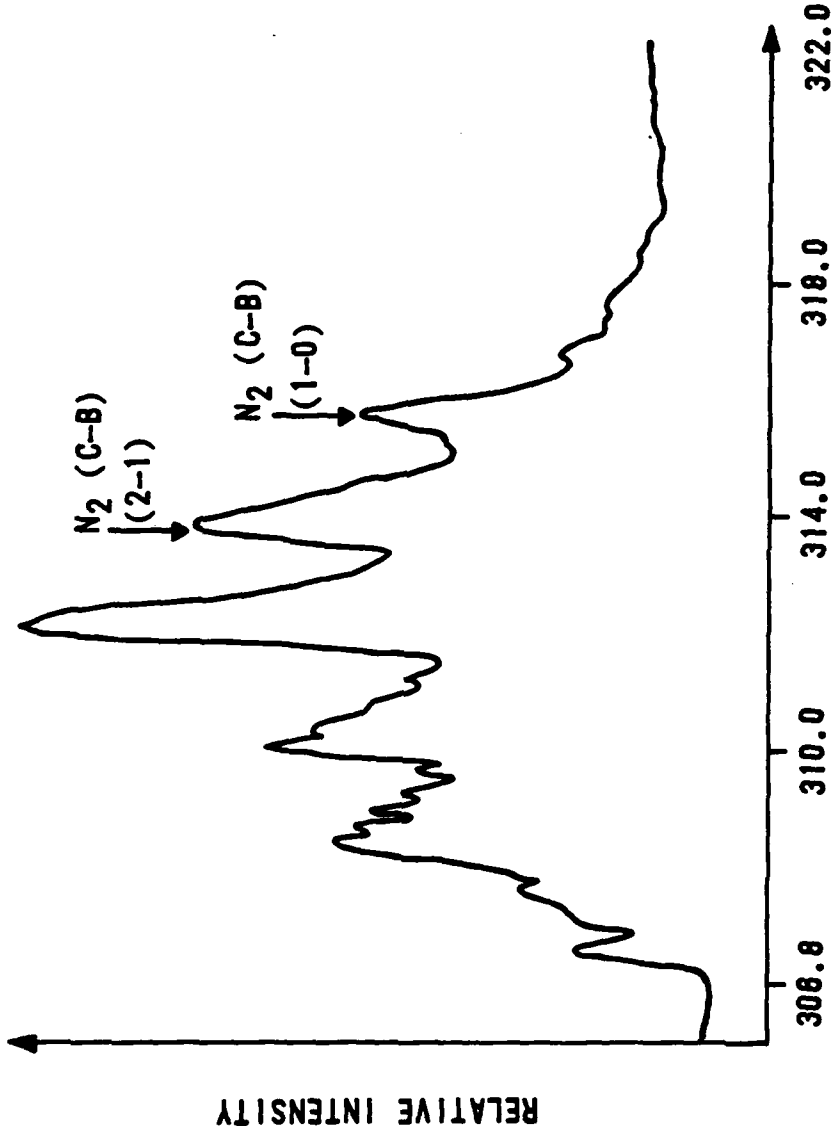

Figure 13. $N_2(C)$ spectrum.

8.0 CONCLUSIONS

The maximum $N_2(A)$ yield obtained through parametric variation was 1×10^{-3}% based upon initial N_2F_4. This corresponded to a concentration of $\sim 2 \times 10^{11}$ molecules/cc, using D_2 in the secondary jets. Similar flow rates using H_2 yielded a 5 to 10 times smaller concentration of $N_2(A)$. The increase with D_2 may be because of the inability of DF to react with $NF(a^1\Delta)$[13] as HF does in the following reactions

$$NF(a^1\Delta) + HF(v' = 2) \rightarrow NF(b^1\Sigma) + HF(v' = 0) \quad (9)$$

$$k = 8.3 \times 10^{-12} \text{ cc/molecule-s}$$

$$NF(a^1\Delta) + HF(v' = 3) \rightarrow NF(b^1\Sigma) + HF(v' = 1) \quad (10)$$

$$k = 7.5 \times 10^{-11} \text{ cc/molecule-s}$$

Therefore, by using D_2 in the reaction sequence the $NF(b^1\Sigma)$ formation from $NF(a^1\Delta)$ is minimized. This provides additional $NF(a^1\Delta)$ for further reaction to form $N_2(A)$. This was checked by comparing the tests with H_2 and tests with D_2. Table 2 contains the flow rate and diagnostic data on these tests. There is a decrease in $NF(b^1\Sigma)$ population as noted by Herbelin and Cohen (Ref. 12). However, the decrease in $NF(b^1\Sigma)$ is insufficient to account for the increase in $NF(a^1\Delta)$ and thus $N_2(A)$. The conclusion is that there is increased jet penetration at similar molar flow rates if H_2 and D_2 because of the higher molecular weight of D_2. The $N_2(A)$ production is then aided by better mixing. The decrease in NF(b) most probably aides $N_2(A)$ but to a lesser degree. The overall conclusion is that D_2 should be used as the secondary gas instead of H_2. A small number of tests were attempted using trip jet injection of D_2 and secondary jet injection of N_2F_4. The result was lower $N_2(B)$ emission at the same flow rates and reversed injection.

TABLE 2. SAMPLE HIGH [$N_2(B)$] TESTS

25% F_2[a] in He	D_2[a] Combustor	D_2[a] Secondary	He[a] Secondary	N_2F_4[a]	P_{cavity} (Torr)[c]	$N_2(B)$ (molecule/cc)
0.167[b]	0.0095	0.02	----	0.26	12.2	1.6×10^{11}
0.152	0.0066	0.02	0.024	0.25	10.4	1.1×10^{11}
0.155	0.0077	0.02	0.085	0.26	13.4	1.3×10^{11}

[a] All flows are in g/s

[b] This test used 35 percent F_2 in He

[c] Torr = 1.33×10^2 Pa (Nm^{-2})

9.0 RECOMMENDATIONS

Further nozzle development is needed to improve mixing. The BCL-16 type nozzle is insufficient for this reaction scheme. It is recommended here that a new nozzle be designed to deal with the very heavy NF_2 and extremely light D_2 penetration problems.

The other question remaining is - what is the actual branching ratio for $NF(a^1\Delta)$ production given by Equation 3. The measurement needs to be made precisely. Previous assumptions of a 90 percent branching ratio were based upon an indirect measurement (Ref. 10). Current research should be directed towards better defining the branching ratio.

Since the pooling rate for $N_2(A)$ is rapid, there will be a limit to the $[N_2(A)]$ which is achievable. Therefore, it is important to find an energy transfer acceptor which may be premixed with the NF_2 or injected early in the reaction sequence. The difficulty lies in finding an acceptor atom or molecule which does not seriously impact the $N_2(A)$ production scheme.

Overall, $N_2F_4 + D_2$ reaction scheme for $N_2(A)$ production holds promise although difficulties have been determined. A program to adequately address these problems may allow for successful use of this scheme for a chemical transfer laser.

REFERENCES

1. Kolts, J.H., Brashears, H.C., and Setser, D.W., J. Chem. Phys., 67, 2931 (1977).

2. Young, R.A. and St. John, G.A., J. Chem. Phys., 48, 895 (1968).

3. Cheah, C.T., Clyne, M.A.A., and Whitefield, P.D., J. C. S. Faraday II, 76, 711 (1980).

4. Tregay, G.W., et al., DF/HF Chemical Laser Technology, Bell Aerospace Textron Report No. D9276-9270003, Bell Aerospace Textron, Buffalo, New York, January 1981.

5. Jones, Y. D., et al., $NF(a^1\Delta)$ Production in a Supersonic Flow Using $N_2F_4 + H_2$ in a BCL-16 Nozzle, AFWL-TR-87-24, Kirtland AFB, New Mexico, January 1988.

6. Rapagnani, N.L. and Davis, S.J., AIAA Journal, 17, 1402 (1979).

7. Jones, Y.D., An Absolute Scanning $NF(a^1\Delta)$ and $NF(b^1\Sigma)$ Diagnostic for the $N_2F_4 + H_2$ System, AFWL-TR-86-99, Kirtland AFB, New Mexico, July 1987.

8. Hays, G.N. and Oskam, H.J., J. Chem. Phys., 59, 6088 (1973).

9. Khakoo, M.A. and Srivastave, S.K., J. Quant Spectrosc. Radiat. Transfer, 30, 31 (1983).

10. Malins, R.J. and Setser, D.W., J. Phys Chem., 85, 1342 (1981).

11. Lofthus, A. and Krupenie, P.H., J. Phys and Chem Ref. Data, 6, 113 (1977).

12. Herbelin, J.M. and Cohen, N., Chem Phys. Lett., 20, 605, (1973).

APPENDIX

REACTIONS IN THE NF_2 + H PRODUCTION OF $N_2(A^3\Sigma_u^+)$

TABLE 1A.

PRINCIPLE REACTIONS AND KNOWN RATES
(All rates are in cc/molecule - s)

1. $NF_2 + H \rightarrow NF(a^1\Delta) + HF(v'= 0,1,2,3)$

   $k_{v'=0} = 9.56 \times 10^{-12}$; $k_{v'=1} = 3.97 \times 10^{-12}$; $k_{v'=2} = 1.03 \times 10^{-12}$; $k_{v'=3} = 1.47 \times 10^{-13}$ Ref. 1,2

2. $NF_2 + H \rightarrow NF(b^1\Sigma) + HF(v'=0)$

   $k_2 = 2.94 \times 10^{-13}$ Ref. 2

3. $NF(a^1\Delta) + H \rightarrow N(^2D) + HF(v'= 0,1,2)$

   $k_3 = 2.5 \times 10^{-13}$ Ref. 3

4. $NF(a^1\Delta) + N(^2D) \rightarrow N_2(B) + F$

   $k_4 = 3.0 \times 10^{-11}$ Ref. 4

5. $NF(a^1\Delta) + HF(v = 2,3) \rightarrow NF(b^1\Sigma) + HF(v'=0,1)$

   $k_{v'=2} = 8.3 \times 10^{-12}$; $k_{v'=3} = 7.5 \times 10^{11}$ Ref. 5

6. $NF(a^1\Delta) + M \rightarrow NF(X^3\Sigma) + M$

   $k_6 = 1.7 \times 10^{-13}$ Ref. 6

7. $NF(b^1\Sigma) + M \rightarrow NF(a^1\Delta) + M$

   $k_7 = 5.0 \times 10^{-12}$ Ref. 6

8. $NF(b^1\Sigma) + M \rightarrow NF(X^3\Sigma) + M$

   $k_8 = 5.0 \times 10^{-12}$ Ref. 6

9. $N(^2D) + N_2(^1\Sigma) \rightarrow N(^4S) + N_2(X)$

   $k_9 = 1.0 \times 10^{-14}$ Ref. 7

10. $N(^2D) + N(^4S) \rightarrow 2N(^4S)$

    $k_{10} = 1.0 \times 10^{-14}$ estimated

11. $2NF(X^3\Sigma) \rightarrow N_2(X) + 2F$

    $k_{11} = 7 \times 10^{-11}$ Ref. 1

12. $NF(a^1\Delta) + NF(X^3\Sigma) \rightarrow N2(X) + 2F$

    $k_{12} = 7 \times 10^{-11}$ Ref. 1

13. $2N_2(A) \rightarrow N_2(B) + N_2(X,V'>0)$

$k_{13} = 1.1 \times 10^{-9}$ Ref. 8

14. $2N_2(A) \rightarrow N_2(C) + N_2(X,V'>0)$

$k_{14} = 2.6 \times 10^{-10}$ Ref. 9

15. $2N_2(A) \rightarrow N_2(C^1) + N_2(X)$

$k_{15} = 2.6 \times 10^{-11}$ Ref. 8

16. $N_2(A) + N(^4S) \rightarrow N_2(X,V'>0) + N(^2P)$

$k_{16} = 3.5 \times 10^{-11}$ Ref. 10

17. $N_2(A) + N(^4S) \rightarrow N_2(X) + N(^2D,^4S)$

$k_{17} = 3.5 \times 10^{-11}$ Ref. 10

18. $N_2(B) + N_2(X) \rightarrow N_2(A,X) + N_2(X)$

$k_{18} = 2.7 \times 10^{-11}$ Ref. 11

REFERENCES

1. Cheah, C.T., Clyne, M.A.A. and Whitefield, P.D., J. C. S. Faraday II, 76, 711 (1980).

2. Malins, R.J. and Setser, D.W., J. Phys. Chem., 85, 1342 (1981).

3. Cheah, C.T. and Clyne, M.A.A., J. Photochem, 15, 21 (1981).

4. Cheah, C.T. and Clyne, M.A.A., J. C. S. Faraday II, 76, 1543 (1980).

5. Herbelin, J.M., Dwok, M.A. and Cohen, N., Modeling of the H + NF_2 Reactive Flow, 5D-TR-81-21, The Aerospace Corporation, El Segundo, California, April 1981.

6. Kwok, M.A., Herbelin, J.M. and Cohen, N., Collisional Quenching and Radiative Decay Studies of $NF(a^1\Delta)$ and $NF(b^1\Sigma^+)$, SAMSO-TR-77-73, The Aerospace Corporation, El Segundo, California, April 1977.

7. Lin, C.L. and Kaufman, F., J. Chem. Phys., 55, 3760 (1971).

8. Hays, G.N. and Oskam, H.J., J. Chem. Phys., 59, 1507 (1973).

9. Hays, G.N. and Oskam, H.J., J. Chem. Phys., 59, 6088 (1973).

10. Vedaud, P.H., Wayne, R.P., Yaron, M. and von Engel, A., J. C. S. Faraday Trans II, 73, 1185 (1976).

11. Young, R.A., Black, G. and Slanger, T.G., J. Chem Phys, 50, 303 (1969).

END

DATE

FILMED

8-88

DTIC